



Research Paper

Magnetic resonance imaging (MRI) of pharmacological ascorbate-induced iron redox state as a biomarker in subjects undergoing radio-chemotherapy



Cameron M. Cushing^{a,1}, Michael S. Petronek^{a,1}, Kellie L. Bodeker^a, Sandy Vollstedt^a, Heather A. Brown^a, Emyleigh Opat^a, Nancy J. Hollenbeck^a, Thomas Shanks^a, Daniel J. Berg^b, Brian J. Smith^h, Mark C. Smith^a, Varun Monga^b, Muhammad Furqan^b, Matthew A. Howardⁱ, Jeremy D. Greenleeⁱ, Kranti A. Mapuskar^a, Joel St-Aubin^a, Ryan T. Flynn^a, Joseph J. Cullen^{d,e,f,g}, Garry R. Buettner^a, Douglas R. Spitz^a, John M. Buatti^a, Bryan G. Allen^{a,*}, Vincent A. Magnotta^{c,**}

^a Free Radical and Radiation Biology Program, Department of Radiation Oncology, Holden Comprehensive Cancer Center, University of Iowa Hospitals and Clinics, USA

^b Division of Hematology and Oncology, Department of Internal Medicine, Holden Comprehensive Cancer Center, University of Iowa Hospitals & Clinics, Iowa City, IA, USA

^c Department of Radiology, Holden Comprehensive Cancer Center, University of Iowa Hospitals and Clinics, USA

^d Department of Surgery, University of Iowa College of Medicine, Iowa City, IA, USA

^e Department of Radiation Oncology, University of Iowa College of Medicine, Iowa City, IA, USA

^f Holden Comprehensive Cancer Center, Iowa City, IA, USA

^g Veterans Affairs Medical Center, Iowa City, IA, USA

^h Department of Biostatistics, Holden Comprehensive Cancer Center, The University of Iowa, Iowa City, IA, USA

ⁱ Department of Neurosurgery, University of Iowa Hospitals & Clinics, Iowa City, IA, USA

ARTICLE INFO

Keywords:

Quantitative imaging

GBM

T2*

QSM

Pharmacological ascorbate

ABSTRACT

Pharmacological ascorbate (P-AscH⁻) combined with standard of care (SOC) radiation and temozolomide is being evaluated in a phase 2 clinical trial (NCT02344355) in the treatment of glioblastoma (GBM). Previously published data demonstrated that paramagnetic iron (Fe³⁺) catalyzes ascorbate's oxidation to form diamagnetic iron (Fe²⁺). Because paramagnetic Fe³⁺ may influence relaxation times observed in MR imaging, quantitative MR imaging of P-AscH⁻-induced changes in redox-active Fe was assessed as a biomarker for therapy response.

Gel phantoms containing either Fe³⁺ or Fe²⁺ were imaged with T2* and quantitative susceptibility mapping (QSM). Fifteen subjects receiving P-AscH⁻ plus SOC underwent T2* and QSM imaging four weeks into treatment. Subjects were scanned: pre-P-AscH⁻ infusion, post-P-AscH⁻ infusion, and post-radiation (3–4 h between scans). Changes in T2* and QSM relaxation times in tumor and normal tissue were calculated and compared to changes in Fe³⁺ and Fe²⁺ gel phantoms. A GBM mouse model was used to study the relationship between the imaging findings and the labile iron pool.

Phantoms containing Fe³⁺ demonstrated detectable changes in T2* and QSM relaxation times relative to Fe²⁺ phantoms. Compared to pre-P-AscH⁻, GBM T2* and QSM imaging were significantly changed post-P-AscH⁻ infusion consistent with conversion of Fe³⁺ to Fe²⁺. No significant changes in T2* or QSM were observed in normal brain tissue. There was moderate concordance between T2* and QSM changes in both progression free survival and overall survival. The GBM mouse model showed similar results with P-AscH⁻ inducing greater changes in tumor labile iron pools compared to the normal tissue.

Conclusions: T2* and QSM MR-imaging responses are consistent with P-AscH⁻ reducing Fe³⁺ to Fe²⁺, selectively in GBM tumor volumes and represent a potential biomarker of response. This study is the first application using MR imaging in humans to measure P-AscH⁻-induced changes in redox-active iron.

* Corresponding author. Department of Radiation Oncology, 200 Hawkins Drive, 01621, PFPW, Iowa City, IA, 52242, USA.

** Corresponding author. Department of Radiology, L311 PBDB, 169 Newton Road, Iowa City, IA, 52242, USA.

E-mail addresses: bryan-allen@uiowa.edu (B.G. Allen), Vincent-magnotta@uiowa.edu (V.A. Magnotta).

¹ Cushing and Petronek contributed equally to this manuscript.

<https://doi.org/10.1016/j.redox.2020.101804>

Received 18 August 2020; Received in revised form 29 October 2020; Accepted 13 November 2020

Available online 19 November 2020

2213-2317/© 2020 The Authors.

Published by Elsevier B.V. This is an open access article under the CC BY-NC-ND license

(<http://creativecommons.org/licenses/by-nc-nd/4.0/>).

1. Introduction

Pharmacological ascorbate (P-AscH⁻), defined as IV administered gram-doses (≈ 5 g–100 g) of ascorbate yielding millimolar concentrations in blood, has re-emerged as a promising adjuvant to chemotherapy and radiation therapy for the treatment of multiple cancers. Phase I clinical trials have established the safety of P-AscH⁻ in pancreatic cancer [1,2], non-small cell lung cancer [3], glioblastoma [3], and ovarian cancer [4]. Pre-clinical studies have demonstrated that ascorbate is selectively toxic to tumor cells and likely synergizes with radiation and chemotherapy agents to improve cancer cell killing [5–7].

The interaction of ascorbate with the labile iron pool (LIP) is one proposed mechanism of P-AscH⁻'s selective cancer cell killing [3,5,8,9]. The LIP is weakly bound and easily chelated, hence called the chelatable iron pool [9–11]. The LIP is one of several pools in which iron resides and represents a small fraction of the total iron within the cell. The magnitude of the LIP in normal tissue is estimated to range from 0.2 to 5 μ M [9,10,12–14]. Unlike iron bound in ferritin or transferrin, the LIP can undergo redox cycling leading to biological activity that can be harnessed for enhancing tumor response [3,20]. The LIP is proposed to catalyze the oxidation of ascorbate, leading to a high flux of hydrogen peroxide [6,15–20] while Fe³⁺ is reduced to Fe²⁺. Fe²⁺ can then undergo cytotoxic reactions, including reactions with molecular oxygen, generating superoxide and hydrogen peroxide or directly initiate oxidation reactions via Fe²⁺-O₂ complexes or the Fenton reaction, (Fe²⁺ + H₂O₂ → Fe³⁺ + OH⁻ + HO*) leading to oxidation of many biomolecules [21–23]. The ability of the LIP to redox cycle has been shown *in vitro* to modify the survival of P-AscH⁻ treated cancer cells [3,5]. Chelation of the LIP during ascorbate treatment with EDTA decreases cancer cell survival via an increase in iron redox cycling [3,5]. In contrast chelation with deferoxamine, increases cancer cell survival during ascorbate treatment via a decrease in the redox cycling of iron [3, 5]. Iron redox cycling is thought to be greater in cancer *versus* normal cells, due to higher baseline cancer cell LIPs than normal cells [3,9].

Detecting changes in the LIP induced by P-AscH⁻ may serve as a biomarker to predict response. Currently, the *in vivo* LIP can be determined following a biopsy with tissue samples analyzed by EPR [9] or a calcein-based assay [24]. However, biopsies are invasive and entail risk to the patient or involve terminal experiments in pre-clinical models, making repeated measurements difficult. These challenges justify the development of non-invasive methods for monitoring the redox state of the LIP as a potential biomarker for response. Two MRI methods, T2* relaxation mapping and quantitative susceptibility mapping (QSM), have shown sensitivity to the total iron concentrations *in vivo* [25–30]. QSM utilizes the phase of the MR signal to estimate the magnetic susceptibility of tissue, as opposed to T2* which utilizes the magnitude of the signal [31–33]. Like T2*, QSM is sensitive to iron concentrations *in vitro* and *in vivo* [25,28–31,34–36]. However, the ability of these approaches to interrogate the LIP *in vivo* is unknown.

The highly paramagnetic properties and strong magnetic moment of Fe³⁺ relative to Fe²⁺ influence T2* relaxation and tissue susceptibility (QSM) [37–39]. Previous work has demonstrated that Fe³⁺ exhibits greater susceptibility leading to substantially shorter relaxation times than Fe²⁺ [26]. Conversion of Fe³⁺ to Fe²⁺ within a tumor is hypothesized to result in a measurably longer T2* relaxation time or lower tissue magnetic susceptibility in QSM, allowing for the *in vivo* monitoring of redox changes in the LIP.

The goal of this study was to assess the feasibility of monitoring acute changes in T2* and QSM changes (within hours) in GBM tumors treated with P-AscH⁻. We show that T2* and QSM imaging can detect changes in the concentration of Fe³⁺ in the physiologic range. These data could be used for quantitation of *in vivo* measurements. We then demonstrate the reliability of T2* and QSM measurements in healthy subjects and GBM patients undergoing standard of care therapy combined with P-AscH⁻. Next, we show that T2* relaxation time increases and QSM decreases in tumors acutely after IV administration of P-AscH⁻ suggesting this

approach could be used to follow changes in the LIP as a biomarker of tumor response. Finally, an animal model is used to quantify changes in the labile iron pool as a result of administration of P-AscH⁻ and the association with quantitative MRI changes.

2. Materials and methods

2.1. Phantom study

To demonstrate that T2* relaxation and QSM have differential responses to equimolar concentrations of Fe³⁺ and Fe²⁺, phantoms containing physiologically relevant iron concentrations (1–100 μ M) were generated. Fe²⁺ stock was made containing 1 mM ferrous sulfate, and 2 mM ferrozine. Ferrozine is an Fe²⁺ chelator that maintains Fe²⁺ in the low spin state. Ascorbate reacts with Fe³⁺ present in the sample to form Fe²⁺ that can then be chelated by ferrozine. Because ascorbate and ferrozine are in excess compared to Fe²⁺, Fe³⁺ is expected to be rapidly reduced and chelated by ferrozine. Fe³⁺ stock was made using 1 mM ferric nitrate and left unchelated. A stock 1% weight to volume low temperature agarose gel was prepared. Agar was divided into two stocks; 1 mM ascorbate was added to one stock (for Fe²⁺) samples. After overnight incubation, appropriate amounts of iron stocks and chelator stocks were combined in 15 mL plastic tubes to achieve the desired concentrations of Fe³⁺ and Fe²⁺: 0, 5, 10, 20, 30, 40, 50, 60, 70, 80, 90, and 100 μ M. Falcon tubes were placed in a water bath doped with 1 mL/L Magnevist and imaged using a 3T TIM TRIO MR system (Siemens, Erlangen Germany) using a multi-echo gradient-echo pulse sequence (TE = 7, 14, 21, 28, 35, 42, 49, and 56 ms; TR = 80 ms; matrix size = 192 × 250; FOV = 200 × 200 mm; slice thickness = 4 mm, flip angle = 7°).

T2* map generation: Quantitative T2* maps were generated by fitting a mono-exponential decay equation to the multi-echo gradient-echo magnitude images by least squares regression.

Quantitative susceptibility map generation: Quantitative susceptibility maps were generated by using the total generalized variation QSM (TGV-QSM) [30]. The code is graciously provided on the Langkammer group's website (<http://www.neuroimaging.at/pages/qsm.php> as accessed 2019-10-14).

2.2. Mouse study

All animal experiments complied with the National Institutes of Health guide for the care and use of laboratory animals (NIH Publications No. 8023, revised 1978).

2.3. Orthotopic mouse injections

U87 GBM cells were cultured in DMEM-F12 media (15% FBS, 1% penicillin-strep, 1% Na-pyruvate, 1.5% HEPES, 0.1% insulin, and 0.02% fibroblast growth factor) and grown to 70–80% confluence at 21% O₂. Before injection, cells were trypsinized and the pellet resuspended in 5% methylcellulose. Three female nude athymic (NU/J) mice (Jackson Labs) were anesthetized using a ketamine (87.5 mg mL⁻¹) xylazine (12.5 mg mL⁻¹) cocktail per the University of Iowa IACUC (Protocol #7111207). Following anesthesia, a 1 cm incision was made to expose the skull and a burr hole was made approximately 3 mm lateral (right) and 2 mm posterior to the bregma. A syringe containing cells was inserted 3 mm deep to the burr hole and 4 × 10⁵ cells in 4 μ L were injected over 1 min. Following completion of the surgery, mice (n = 3) received a 5-day treatment of meloxicam (2 mg kg⁻¹) for pain management. Following confirmation of tumor growth as a hyperintense region on a T2-weighted anatomical image, mice were treated twice daily with ascorbate (4 g kg⁻¹, delivered intraperitoneally) for 7 consecutive days.

2.4. Mouse MR imaging

The mice were imaged on day 0 before the first ascorbate injection and again on day 7. Images were collected on a 7T GE small animal scanner (MR901). T2 weighted anatomical images were collected using a spoiled gradient echo sequence. T2* weighted images were collected using a gradient echo sequence (TR = 68 ms, TE = 2.5, 8.5, 14.5, and 20.5 ms, Flip angle = 16°, FOV = 25 × 20 mm, Slice thickness/gap = 0.4/0.1 mm, matrix = 256 × 204, NEX = 2). T2* maps were generated using a combination of the echo times collected and fitting each voxel to a mono-exponential curve as described for the phantom study. Images were imported into 3D Slicer software where regions of interest corresponding to the tumor and normal tissue were delineated based on the T2-weighted image. The tumor tissue was defined as the entire hyperintense region on the T2-weighted image. A similar volume of normal brain tissue was identified in the contralateral hemisphere.

2.5. EPR spectroscopy

Following euthanasia of the mice, brains were removed from the skull and separated bilaterally into tumor and contralateral normal tissue. Tissues were immediately flash frozen with liquid nitrogen and stored at -80 °C until sample preparation. Samples were prepared and analyzed for LIP concentrations using electron paramagnetic resonance (EPR) using a Bruker EMX by monitoring the high-spin Fe³⁺ ferrioxamine (DFO-Fe³⁺) complex at $g = 4.3$ at 100 K (Bruker ER4111VT variable temperature accessory) as previously described in Refs. [42].

2.6. Statistical analysis

The mean T2* relaxation time of voxels within the delineated region of interest were calculated. Mean T2* relaxation times were compared using a paired, two-tailed *t*-test. For EPR analysis, the mean signal intensity (A.U.) from triplicate measures were used to determine the labile iron concentration of samples based on a standard curve ranging from 0 to 10 μM ferrioxamine. Mean tumor and normal tissue labile iron measures were compared using a paired, two-tailed *t*-test.

2.7. Human studies

The work described has been carried out following The Code of Ethics of the World Medical Association. Informed consent was obtained before subject participation.

2.8. Healthy subject test-retest

Healthy subjects were invited to participate in a study exploring the repeatability of T2* and QSM imaging as an active comparison group. IRB approval was obtained from the University of Iowa Biomedical Institutional Review Board (IRB200810706; Magnotta PI). This human study did not meet [ClinicalTrials.gov](https://www.clinicaltrials.gov) registration criteria. Four normal healthy volunteers (2 male, 2 female) were consented to undergo MR scanning once weekly for four weeks.

Each scan session included two multi-echo gradient-echo sequences (TE = 4, 10, 20, 30, 36, 42, 48, 54, 60, 67, 73, and 79 ms; TR = 4000 ms; matrix size = 192 × 256; FOV = 200 × 200 mm; slice thickness 4 mm) and an anatomical T1 MP-RAGE (TE = 3 ms, TR = 2300 ms, TI = 900 ms, matrix size 256 × 256 × 192, FOV = 256 × 256 × 192 mm). The subjects were repositioned between multi-echo gradient-echo acquisitions.

The multi-echo gradient-echo data were used to generate quantitative T2* maps and QSM maps as described above. The second echo of the acquisition (TE = 10 ms) was used to register the quantitative maps to the T1 image acquired during the same session, which was also registered to the T1 image from the first scan session. Brain regions were parcellated using FreeSurfer [40]. The mean values for T2* relaxation times and magnetic susceptibility from the cerebral white matter were

extracted. Intra-day variation was assessed by linear regression of the mean values from the two scans taken on the same day against each other. The resulting correlation coefficient (R) of the linear regression was calculated for each region. The coefficient of variation is also reported for each region.

2.9. Imaging of subjects with glioblastoma

Subjects participating in the phase 2 clinical trial of P-AscH⁺ for GBM (NCT02344355) could opt-in for T2* MR sequences as an exploratory aim of the study. Fifteen subjects consented to undergo optional imaging and were imaged on a clinical 3T MRI (Siemens TIM TRIO, Erlangen Germany) scanner post-surgery at three time points on boost simulation day (RT fraction 19, 20, or 21, approximately four weeks into trial therapy that included an evening dose of temozolomide followed in the morning by P-AscH⁺ followed by daily radiation). T2* and QSM maps were acquired at the following times on that day: (scan 1) prior to daily therapy; (scan 2) 30–90 min post P-AscH⁺ infusion but prior to radiation treatment; and (scan 3) 4 h post P-AscH⁺ infusion and post radiation ([Supplemental Fig. 1](#)). Additional MR images collected as part of this study included T2 weighted imaging prior to P-AscH⁺ infusion and a fluid attenuated inversion recovery (FLAIR) during the second scan. T1 with contrast was acquired only after the final QSM and T2* images were acquired. Analyzed subjects were followed over time to determine progression free survival (PFS) and overall survival (OS). PFS was determined from the start of treatment to progression or last follow-up with imaging. OS was determined from the start of treatment to death or last medical follow-up.

2.10. Comparison group

GBM subjects not receiving P-AscH⁺ infusions were invited to participate in a study exploring T2* and QSM imaging as an active comparison group. IRB approval was obtained from The University of Iowa Biomedical Institutional Review Board (IRB201708773). This study did not meet [ClinicalTrials.gov](https://www.clinicaltrials.gov) registration criteria. Five patients were consented and were imaged at baseline (*i.e.*, prior to initiating radiation therapy) and at radiation fraction 20 at two time points during each visit: (scan 1) prior to the daily radiation treatment and (scan 2) three to 4 h post radiation treatment.

2.11. Image registration and contouring

The contrast-enhanced T1 weighted images served as the fixed image and the T2* maps, QSM maps, and FLAIR images were co-registered to this image using BRAINSFIT for registration [41]. For the T2* and QSM maps, registration was driven by aligning the second echo from the multi-echo GRE to the contrast enhanced T1 weighted image. The calculated transform was then applied to the T2* and QSM maps. Contours were drawn referencing the FLAIR and contrast enhanced T1 weighted images by an American Board of Radiology certified radiation oncologist. The contours were drawn blinded to the T2* and QSM maps and were eroded (contour taken in) by 2 mm. Voxels with T2* values greater than 250 ms were excluded from the volume.

2.12. Statistical analysis

Quantitative measures of T2* relaxation times and magnetic susceptibility were analyzed by comparing the slopes *via* analysis of covariance (ANCOVA.) Comparisons between mean relaxation times and QSM in normal and tumor tissue at baseline were performed with the Wilcoxon Signed Rank test as were successive time points in each tissue type. (*i.e.* pre-to post P-AscH⁺).

PFS and OS endpoints were compared to normalized T2* relaxation time changes using Harrell's concordance index [43,44]. Tumor T2* relaxation times were normalized by dividing by the contralateral

associated white matter as an internal control. The concordance index (C-index) is interpreted as the proportion of patient pairs whose ordering of observed survival time is concordant with relaxation time changes. A C-index of 0.5 represents no concordance between the biomarker and survival while a C-index of 1.0 represents perfect concordance.

3. Results

3.1. Phantom study

Phantom studies demonstrated the differential response of $T2^*$ for Fe^{3+} compared to Fe^{2+} . Comparing the slopes of the mean relaxation times for Fe^{3+} and Fe^{2+} , Fig. 1A, revealed that on an equimolar basis, Fe^{3+} induced greater change in $T2^*$ (slope = $-186 \mu s \mu M^{-1} Fe^{3+}$) than Fe^{2+} (slope = $-33 \mu s \mu M^{-1} Fe^{2+}$). ANCOVA analysis shows these slopes are significantly different ($F(1,1) = 14.3, p < 0.001$). Physiologic iron concentrations are highlighted on the graph in Fig. 1A.

QSM data from these phantoms show increasing magnetic susceptibility with increasing concentrations of Fe^{3+} (slope = $+0.308$ ppb per $\mu M Fe^{3+}$), Fig. 1B. However, Fe^{2+} had little effect on magnetic susceptibility (slope = -0.041 ppb per $\mu M Fe^{2+}$). The difference in these slopes is statistically significant ($F(1,1) = 7.3, p < 0.001$). These data suggest that differences in Fe^{3+} and Fe^{2+} may be detected by MR imaging at physiologically relevant concentrations. Taken along with the data from $T2^*$ measurements, this phantom experiment suggested that changes in iron redox state may be visible *in vivo*.

3.2. Test-retest study

$T2^*$ imaging has a high degree of correlation between the first and second scans, Fig. 2A. Plotted is the second scan of a two-scan session against the first scan, $R = 0.99$. The coefficient of variation is approximately 0.8%. Using 40 ms as an approximation for the mean value for global $T2^*$ in the brain yields a white matter standard deviation of approximately 0.3 ms. Any change greater than 40 ms is likely due to a true biochemical change.

QSM also showed a high degree of reproducibility, Fig. 2B. The R for cerebral white matter is 0.95. The coefficient of variation is 20%, likely due to many values being so close to zero. Using the measured mean value of -3 ppb, a standard deviation of 0.6 ppb is calculated. As shown below, experimental changes are greater than 0.6 ppb. These results suggest a high level of reproducibility in the scan methods.

3.3. Mouse study

We assessed the underlying mechanism of P-AscH induced signal changes using an orthotopic GBM model. U87 tumors treated with P-AscH revealed a significant change (day 7 versus day 0) in $T2^*$ relaxation times between tumor and normal brain tissue (Supplemental Figure 4A). The change in $T2^*$ relaxation times was 20.3% in the tumor and -3.5% in the contralateral normal brain. In the same study, EPR spectroscopy measurements of tissues obtained from the same mice after the 7-day course of treatment with P-AscH demonstrated a significant difference in the LIP (Supplemental Figure 4B) in the U87 GBM tumors ($1.8 \pm 0.05 \mu M$) as compared to the normal brain tissue ($1.4 \pm 0.08 \mu M$). These EPR results confirmed the observed $T2^*$ changes at 7 days were accompanied by changes in LIP using an independent methodology.

3.4. Clinical study evaluating acute $T2^*$ and QSM changes after P-AscH administration

The hypothesis for this study is that $T2^*$ and QSM can detect acute changes in tumor and normal tissue as a result of administration of P-AscH. Representative images from one subject are shown in Fig. 3. Fig. 3A shows the T1 contrast-enhanced anatomical image with the

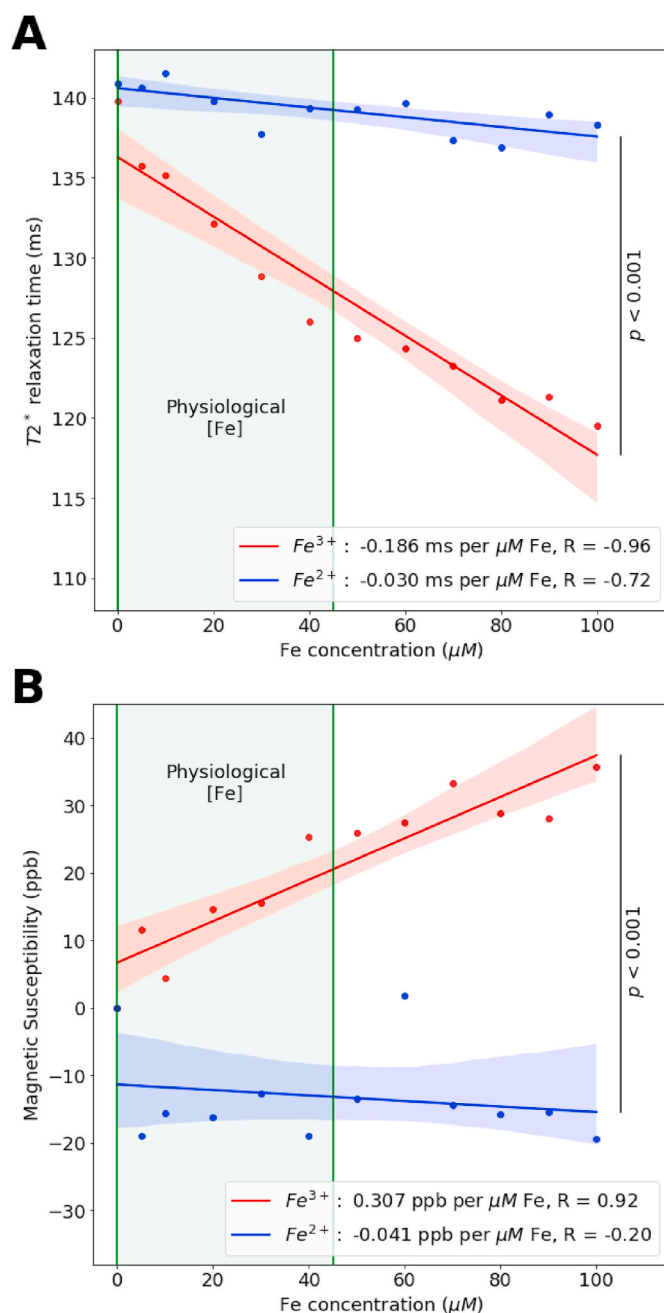


Fig. 1. Fe^{3+} is primarily responsible for changes seen in relaxation rate attributed to iron content. Phantoms were scanned on a Siemens 3T TIM Trio scanner using a multi-echo gradient echo sequence. $T2^*$ relaxation rates (A) were calculated by fitting a mono-exponential decay curve to magnitude images on a voxel-by-voxel basis. Quantitative susceptibility maps (B) were generated using the total generalized variation method of Langkammer et al. [30]. Error bars indicate standard deviation within the tube, shaded bounds are the 95% confidence interval of the linear regression. ANCOVA analysis demonstrates that $T2^*$ relaxation times are statistically significant ($p < 0.001$) as are the slopes QSM ($p < 0.001$). Ferric iron was as the high spin Fe^{3+} complex. Ferrous iron was as the low spin Fe^{2+} (ferrozine)₃ complex.

contrast enhancing region of tumor contoured. Fig. 3B shows a difference map of the $T2^*$ maps generated by subtracting the aligned post-P-AscH map from the pre-P-AscH $T2^*$ map. Difference maps show how the quantitative measures have changed between two successive scans. Red indicates that $T2^*$ relaxation time increased as a result of P-AscH administration (consistent with Fe^{3+} being reduced to Fe^{2+}), blue regions show a decrease in $T2^*$ relaxation time. This subject had an

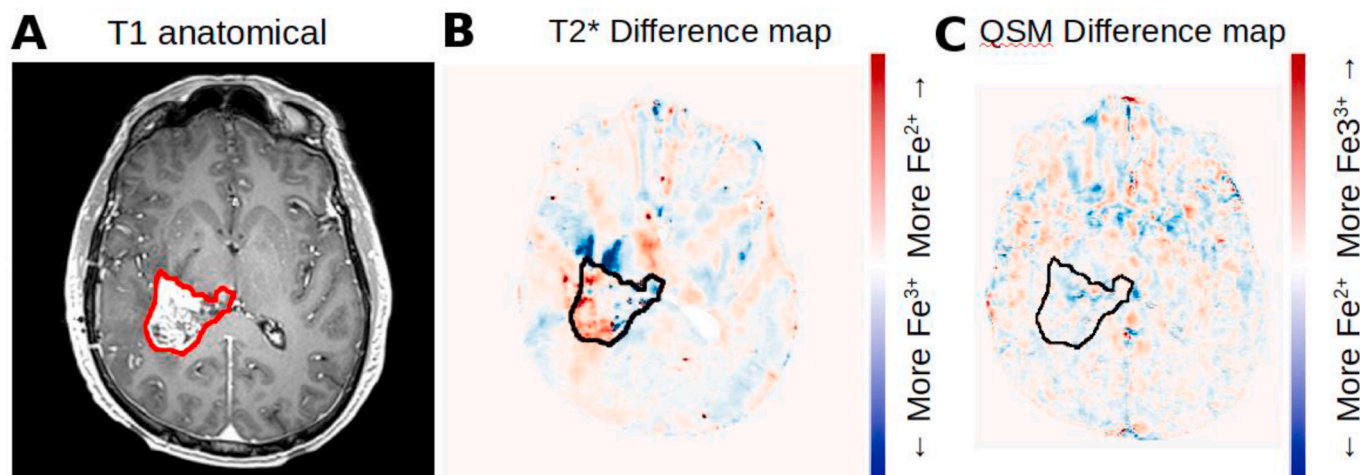


Fig. 3. Representative images of T2* and QSM change as a result of acute P-AscH administration. **A.** T1 contrast enhanced anatomical showing the extent of the contrast enhancing region of tumor (contoured in red). **B.** Difference map (post P-AscH minus pre P-AscH) showing the change in T2* as a result of acute P-AscH administration. Red indicates an increase in T2*, consistent with Fe³⁺ being reduced to Fe²⁺. **C.** Difference map (post P-AscH minus pre P-AscH) showing the change in magnetic susceptibility as a result of acute P-AscH administration. Blue indicates a decrease in magnetic susceptibility, consistent with Fe³⁺ being reduced to Fe²⁺. (For interpretation of the references to color in this figure legend, the reader is referred to the Web version of this article.)

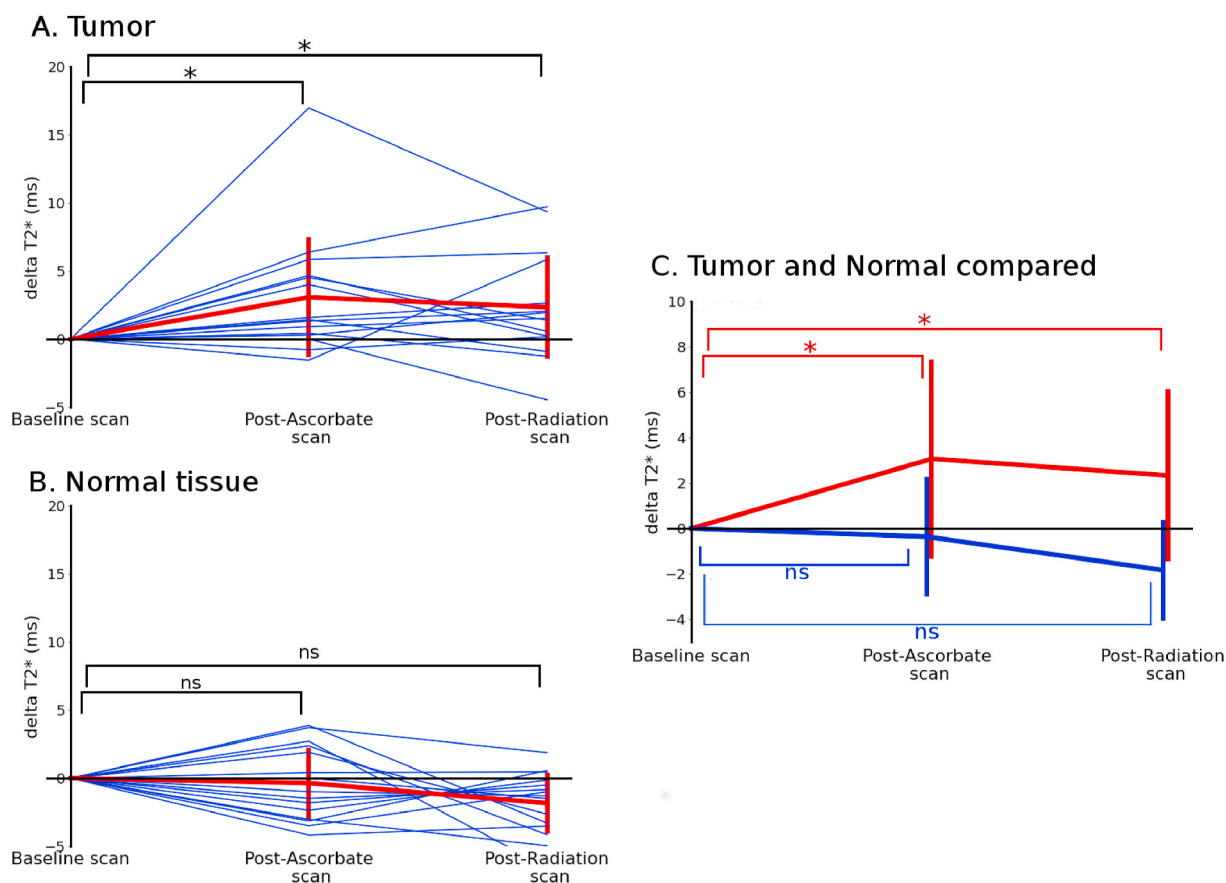


Fig. 4. Time-course of mean T2* values in the contrast enhancing region of tumors (**A**) and normal tissue (**B**) of subjects receiving P-AscH show a persistent change in tumors post P-AscH. T2* is increased by 3.0 ms ($p = 0.007$) compared to baseline post-P-AscH infusion (approximately 4 h post baseline scan and 30 min post infusion) and remains elevated (2.3 ms, $p = 0.02$) post-radiation (approximately 8 h post baseline scan and 3.5 h post infusion). Normal tissue shows no significant changes post-P-AscH infusion (-0.4 ms, $p = 0.65$) and post radiation (-1.4 ms, $p = 0.33$). (**C**) Shows the differences between mean changes observed in contrast enhancing region of tumors and normal tissue. Contrast enhancing region of tumors were contoured on a contrast-enhanced T1 image by a board-certified radiation oncologist. Data are normalized per subject to the baseline scan.

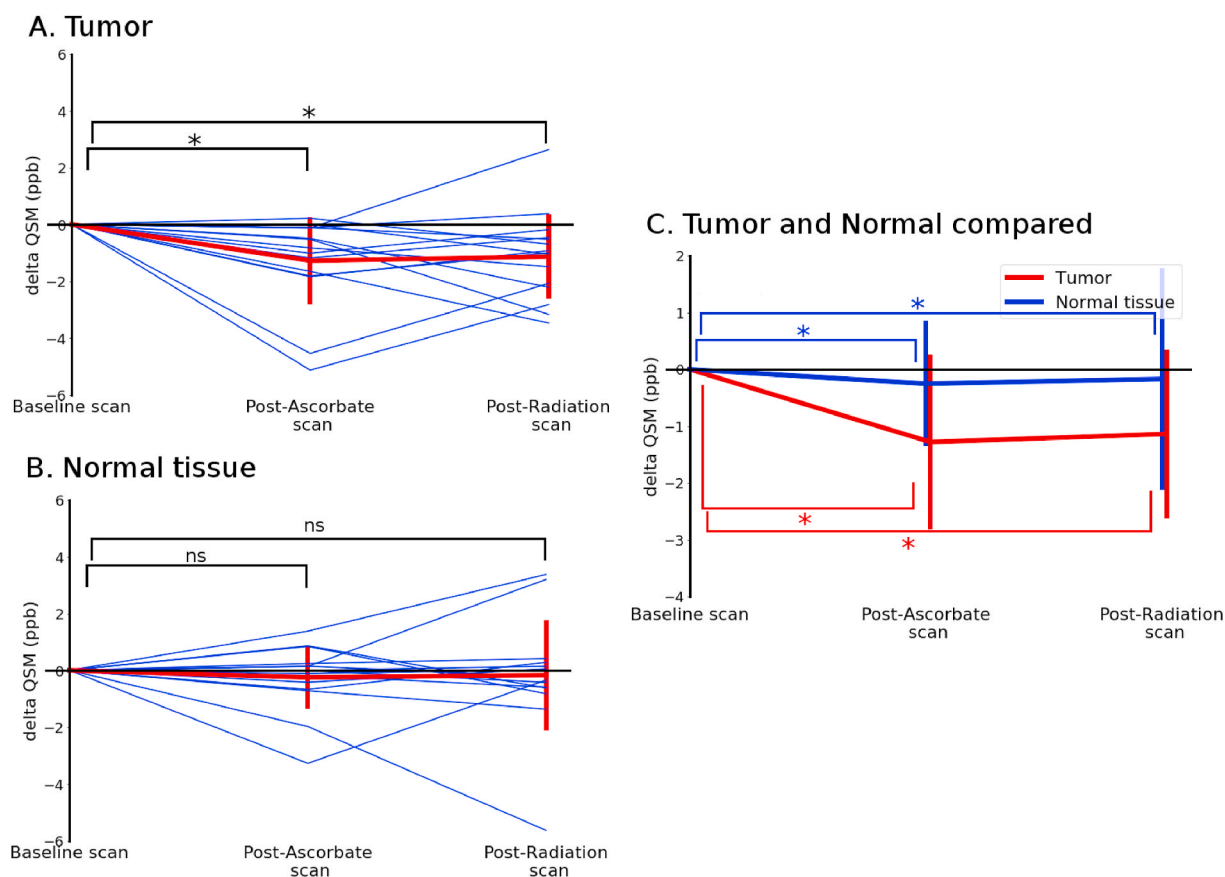


Fig. 5. Time-course of mean QSM values in the contrast enhancing region of tumors (A) and normal tissue (B) of subjects receiving P-AsCH show a persistent change in tumors post P-AsCH. QSM post-P-AsCH infusion is decreased by 1.3 ppb ($p = 0.001$) compared to baseline (approximately 4 h post baseline scan and 30 min post infusion) and remains elevated (1.2 ppb, $p = 0.009$) post-radiotherapy (approximately 8 h post baseline scan and 3.5 h post infusion). Normal tissue showed no significant change post-P-AsCH infusion (-0.28 ppb, $p = 0.65$) or post radiation therapy (-0.19 , $p = 0.39$). (C) Shows the differences between mean changes observed in the contrast enhancing region of tumors and normal tissue. Contrast enhancing region of tumors were contoured on a contrast-enhanced T1 image by a board-certified radiation oncologist. Data are normalized per subject to the baseline scan.

Table 1

Comparison of change in $T2^*$ relaxation times to patient outcomes using Harrell's C-index.

	C-Index	95% CI	p-value
PFS (median = 9.4 mo)			
Total Tumor: Normal	0.527	(0.237, 0.817)	0.85
T1 – Enhancing Region: Normal	0.6	(0.338, 0.862)	0.45
OS (median = 23 mo)			
Total Tumor: Normal	0.605	(0.305, 0.904)	0.49
T1 – Enhancing Region: Normal	0.535	(0.262, 0.807)	0.80

changes in labile iron. Our $T2^*$ phantom studies found the slopes to be $-186 \mu\text{M}^{-1}$ for Fe^{3+} and $-33 \mu\text{M}^{-1}$ for Fe^{2+} . From these slopes, we can estimate the concentration of iron being reduced following P-AsCH administration using the following equation:

[iron reduction] (μM) = $\Delta T2^* \times (\text{slope}_{\text{ferric}} - \text{slope}_{\text{ferrous}})$ The mean change seen in subjects for $T2^*$ was measured to be 3.0 ms, suggesting that approximately 19 μM of ferric iron is being reduced by P-AsCH. Similarly, the same linear analysis can be applied using QSM data. QSM phantom studies indicate slopes of $+0.308$ ppb per μM Fe^{3+} and -0.041 ppb μM^{-1} Fe^{2+} , with a measured change of -1.3 ppb. This equates to approximately 3.7 μM of iron being reduced. The redox-active iron pool in tumors is thought to be on order of 0.5–5 μM [8–10] with transient changes of 20 μM or more possible. In an orthotopic GBM animal model, we observed a similar pattern of selective increases in $T2^*$ relaxation times. When the tumor and adjacent normal tissue was removed, this

revealed significantly more labile iron in the tumor relative to the normal tissue. This supports the hypothesis that $T2^*$ mapping is capable of detecting the selective labilization of iron by P-AsCH.

The proposal that QSM and $T2^*$ may capture *in vivo* changes in the net redox state of iron is a novel and potentially clinically useful result. This study demonstrates how both $T2^*$ and QSM methods may be used to monitor redox metabolic changes caused by manipulating LIPs with a pharmaceutical agent (P-AsCH). The C-index [43,44] shows moderate concordance between the change in tumor relaxation times following P-AsCH administration in both PFS and OS. Statistical significance is not achieved likely due to the small sample size of the current study. This clinical finding suggests that $T2^*$ and QSM mapping has the capacity to provide invaluable data to studies that link iron metabolic perturbations to patient survival [12]. The results are consistent with the hypothesis that $T2^*$ and QSM may be used to assess *in vivo* iron redox metabolism.

This work also describes a differential response in the MR imaging of tumor and normal tissue to P-AsCH. This study is the first to present a method for monitoring the *in vivo* changes in redox-active iron metabolism caused by the direct manipulation of the *endogenous* redox state of iron in cancer subjects. Future work should involve pre-clinical imaging of iron metabolism in orthotopic models and further development of the techniques to analyze the variation of LIP iron within the tumor using direct analytical methodologies.

Authorship

Conception and Design: C.M. Cushing, M.S. Petronek, K.L. Bodeker,

J. St-Aubin, R.T. Flynn, J.J. Cullen, G.R. Buettner, D.R. Spitz, J.M. Buatti, B.G. Allen, V.A. Magnotta.

Development of methodology: C.M. Cushing, M.S. Petronek, K.L. Bodeker, J. St-Aubin, R.T. Flynn, J.J. Cullen, G.R. Buettner, D.R. Spitz, J.M. Buatti, B.G. Allen, V.A. Magnotta.

Acquisition of data (acquired and managed patients, provided facilities, etc.): C.M. Cushing, M.S. Petronek, K.L. Bodeker, S. Vollstedt, H.A. Brown, E. Opat, N. Hollenbeck, T. Shanks, D.J. Berg, M.C. Smith, V. Monga, M.A. Howard, J.D. Greenlee.

Analysis and interpretation of data (e.g., statistical analysis, biostatistics, computational analysis): C.M. Cushing, M.S. Petronek, B.G. Allen, K. Mapuskar, M. Furqan, D.R. Spitz, B.J. Smith, G.R. Buettner, V.A. Magnotta.

Writing, review, and/or revision of the manuscript: C.M. Cushing, M.S. Petronek, K.L. Bodeker, S. Vollstedt, H.A. Brown, E. Opat, N.J. Hollenbeck, T. Shanks, D.J. Berg, B.J. Smith, M.C. Smith, V. Monga, M.A. Howard, J.D. Greenlee, J. St-Aubin, R.T. Flynn, J.J. Cullen, G.R. Buettner, D.R. Spitz, J.M. Buatti, B.G. Allen, V.A. Magnotta.

Administrative, technical, or material support (i.e., reporting or organizing data, constructing databases): K.L. Bodeker, S. Vollstedt, H.A. Brown, E. Opat, N. Hollenbeck, G.R. Buettner, V.A. Magnotta.

Funding

This work was supported by the National Institutes of Health grants P01 CA217797, R01 CA169046, U01 CA140206, R01 CA182804, and T32 CA078586 as well as the Gateway for Cancer Research grant G-17-1500. Core facilities were supported in part by the Carver College of Medicine and the Holden Comprehensive Cancer center, National Institutes of Health P30 CA086862. Core facilities were supported in part by the Carver College of Medicine and the Holden Comprehensive Cancer center, National Institutes of Health (P30CA086862, S10OD025025, and S10RR028821)

Declaration of competing interest

None.

Acknowledgments

The Magnetic Resonance Research Center and the ESR Facility at The University of Iowa as well as the Department of Radiation Oncology provided invaluable support.

Appendix A. Supplementary data

Supplementary data to this article can be found online at <https://doi.org/10.1016/j.redox.2020.101804>.

References

- [1] J.L. Welsh, B.A. Wagner, T.J. van't Erve, P.S. Zehr, D.J. Berg, T.R. Halfdanarson, et al., Pharmacological ascorbate with gemcitabine for the control of metastatic and node-positive pancreatic cancer (PACMAN): results from a phase I clinical trial, *Canc. Chemother. Pharmacol.* 71 (2013) 765–775.
- [2] D.A. Monti, E. Mitchell, A.J. Bazzan, S. Littman, G. Zabrecky, C.J. Yeo, et al., Phase I evaluation of intravenous ascorbic acid in combination with gemcitabine and erlotinib in patients with metastatic pancreatic cancer, *PLoS One* 7 (1) (2012), e29794.
- [3] J.D. Schoenfeld, Z.A. Sibenaller, K.A. Mapuskar, B.A. Wagner, K.L. Cramer-Morales, M. Furqan, et al., O₂— and H₂O₂-mediated disruption of Fe metabolism causes the differential susceptibility of NSCLC and GBM cancer cells to pharmacological ascorbate, *Canc. Cell* 31 (2017) 487–500.e8.
- [4] Y. Ma, J. Chapman, M. Levine, K. Polireddy, J. Drisko, Q. Chen, High-dose parenteral ascorbate enhanced chemosensitivity of ovarian cancer and reduced toxicity of chemotherapy, *Sci. Transl. Med.* 6 (2014), 222ra18–222ra18.
- [5] J.D. Schoenfeld, Z.A. Sibenaller, K.A. Mapuskar, M.D. Bradley, B.A. Wagner, G.R. Buettner, et al., Redox-active metals and H₂O₂ mediate the increased efficacy of pharmacological ascorbate in combination with gemcitabine or radiation in pre-clinical sarcoma models, *Redox Biology* 14 (2018) 417–422.
- [6] J. Du, J.J. Cullen, G.R. Buettner, Ascorbic acid: chemistry, biology and the treatment of cancer, *Biochim. Biophys. Acta* 1826 (2012) 443–457.
- [7] M.G. Espey, P. Chen, B. Chalmers, J. Drisko, A.Y. Sun, M. Levine, et al., Pharmacologic ascorbate synergizes with gemcitabine in preclinical models of pancreatic cancer, *Free Radic. Biol. Med.* 50 (2011) 1610–1619.
- [8] J. Du, B.A. Wagner, G.R. Buettner, J.J. Cullen, Role of labile iron in the toxicity of pharmacological ascorbate, *Free Radic. Biol. Med.* 84 (2015) 289–295.
- [9] J.C. Moser, M. Rawal, B.A. Wagner, J. Du, J.J. Cullen, G.R. Buettner, Pharmacological ascorbate and ionizing radiation (IR) increase labile iron in pancreatic cancer, *Redox Biol* 2 (2013) 22–27.
- [10] M.S. Petronek, D.R. Spitz, G.R. Buettner, B.G. Allen, Linking cancer metabolic dysfunction and genetic instability through the lens of iron metabolism, *Cancers* 11 (8) (2019) 1077.
- [11] F. Petrat, H de Groot, R. Sustmann, U. Rauen, The chelatable iron pool in living cells: a methodically defined quantity, *Biol. Chem.* 383 (2005) 489–502.
- [12] J. Jian, Q. Yang, J. Dai, J. Eckard, D. Axelrod, J. Smith, et al., Effects of iron deficiency and iron overload on angiogenesis and oxidative stress—a potential dual role for iron in breast cancer, *Free Radic. Biol. Med.* 50 (2011) 841–847.
- [13] Y. Ma, H. de Groot, Z. Liu, R.C. Hider, F. Petrat, Chelation and determination of labile iron in primary hepatocytes by pyridinone fluorescent probes, *Biochem. J.* 395 (2006) 49–55.
- [14] G.R. Greenberg, M.M. Wintrobe, A labile iron pool, *J. Biol. Chem.* 165 (1946) 397–398.
- [15] Q. Chen, M.G. Espey, M.C. Krishna, J.B. Mitchell, C.P. Corpe, G.R. Buettner, et al., Pharmacologic ascorbic acid concentrations selectively kill cancer cells: action as a pro-drug to deliver hydrogen peroxide to tissues, *Proc. Natl. Acad. Sci. U. S. A.* 102 (2005) 13604–13609.
- [16] Q. Chen, M.G. Espey, A.Y. Sun, J.-H. Lee, M.C. Krishna, E. Shacter, et al., Ascorbate in pharmacologic concentrations selectively generates ascorbate radical and hydrogen peroxide in extracellular fluid in vivo, *Proc. Natl. Acad. Sci. U. S. A.* 104 (2007) 8749–8754.
- [17] Q. Chen, M.G. Espey, A.Y. Sun, C. Pooput, K.L. Kirk, M.C. Krishna, et al., Pharmacologic doses of ascorbate act as a prooxidant and decrease growth of aggressive tumor xenografts in mice, *Proc. Natl. Acad. Sci. U. S. A.* 105 (2008) 11105–11109.
- [18] C.M. Doskey, V. Buranasudja, B.A. Wagner, J.G. Wilkes, J. Du, J.J. Cullen, et al., Tumor cells have decreased ability to metabolize H₂O₂: implications for pharmacological ascorbate in cancer therapy, *Redox Biol* 10 (2016) 274–284.
- [19] C. Klinghoffer, U. Kämmerer, M. Koospal, B. Mühling, M. Schneider, M. Kapp, et al., Natural resistance to ascorbic acid induced oxidative stress is mainly mediated by catalase activity in human cancer cells and catalase-silencing sensitizes to oxidative stress, *BMC Compl. Alternative Med.* 12 (2012) 61.
- [20] K.E. Olney, J. Du, T.J. van't Erve, J.R. Witmer, Z.A. Sibenaller, B.A. Wagner, et al., Inhibitors of hydroperoxide metabolism enhance ascorbate-induced cytotoxicity, *Free Radic. Res.* 47 (2013) 154–163.
- [21] G.R. Buettner, B.A. Jurkiewicz, Catalytic metals, ascorbate and free radicals: combinations to avoid, *Radiat. Res.* 145 (1996) 532–541.
- [22] S.Y. Qian, G.R. Buettner, Iron and dioxygen chemistry is an important route to initiation of biological free radical oxidations: an electron paramagnetic resonance spin trapping study, *Free Radic. Biol. Med.* 26 (1999) 1447–1456.
- [23] B.A. Wagner, G.R. Buettner, C.P. Burns, Free radical-mediated lipid peroxidation in cells: oxidizability is a function of cell lipid bis-allylic hydrogen content, *Biochemistry* 33 (1994) 4449–4453.
- [24] S. Epsztejn, O. Kakhlon, H. Glickstein, W. Breuer, Z.I. Cabantchik, Fluorescence analysis of the labile iron pool of mammalian cells, *Anal. Biochem.* 248 (1997) 31–40.
- [25] C. Ghadery, L. Pirpamer, E. Hofer, C. Langkammer, K. Petrovic, M. Loitfelder, et al., R₂* mapping for brain iron: associations with cognition in normal aging, *Neurobiol. Aging* 36 (2015) 925–932.
- [26] K. Ghassaban, S. Liu, C. Jiang, E.M. Haacke, Quantifying iron content in magnetic resonance imaging, *Neuroimage* 187 (2019) 77–92.
- [27] P.A. Hardy, D. Gash, R. Yokel, A. Andersen, Y. Ai, Z. Zhang, Correlation of R₂ with total iron concentration in the brains of rhesus monkeys, *J. Magn. Reson. Imag.* 21 (2005) 118–127.
- [28] C. Langkammer, N. Krebs, W. Goessler, E. Scheurer, F. Ebner, K. Yen, et al., Quantitative MR imaging of brain iron: a postmortem validation study, *Radiology* 257 (2010) 455–462.
- [29] C. Langkammer, F. Schweser, N. Krebs, A. Deistung, W. Goessler, E. Scheurer, et al., Quantitative susceptibility mapping (QSM) as a means to measure brain iron? A post mortem validation study, *Neuroimage* 62 (2012) 1593–1599.
- [30] C. Langkammer, K. Bredies, B.A. Poser, M. Barth, G. Reishofer, A.P. Fan, et al., Fast quantitative susceptibility mapping using 3D EPI and total generalized variation, *Neuroimage* 111 (2015) 622–630.
- [31] S.-Q. Yan, J.-Z. Sun, Y.-Q. Yan, H. Wang, M. Lou, Evaluation of brain iron content based on magnetic resonance imaging (MRI): comparison among phase value, R₂* and magnitude signal intensity, *PLoS One* 7 (2012), e31748.
- [32] T. Liu, P. Spincemaille, L. de Rochefort, B. Kressler, Y. Wang, Calculation of susceptibility through multiple orientation sampling (COSMOS): a method for conditioning the inverse problem from measured magnetic field map to susceptibility source image in MRI, *Magn. Reson. Med.* 61 (2009) 196–204.
- [33] T. Liu, C. Wisniewski, M. Lou, W. Chen, P. Spincemaille, Y. Wang, Nonlinear formulation of the magnetic field to source relationship for robust quantitative susceptibility mapping, *Magn. Reson. Med.* 69 (2013) 467–476.
- [34] A. Deistung, A. Schäfer, F. Schweser, U. Biedermann, R. Turner, J.R. Reichenbach, Toward in vivo histology: a comparison of quantitative susceptibility mapping

- (QSM) with magnitude-, phase-, and R2*-imaging at ultra-high magnetic field strength, *Neuroimage* 65 (2013) 299–314.
- [35] E.M. Haacke, S. Liu, S. Buch, W. Zheng, D. Wu, Y. Ye, Quantitative susceptibility mapping: current status and future directions, *Magn. Reson. Imag.* 33 (2015) 1–25.
- [36] Y. Wang, P. Spincemaille, Z. Liu, A. Dimov, K. Deh, J. Li, et al., Clinical quantitative susceptibility mapping (QSM): biometal imaging and its emerging roles in patient care, *J. Magn. Reson. Imag.* 46 (2017) 951–971.
- [37] B. Cohen, H. Dafni, G. Meir, A. Harmelin, M. Neeman, Ferritin as an endogenous MRI reporter for noninvasive imaging of gene expression in C6 glioma tumors, *Neoplasia* 7 (2005) 109–117.
- [38] S.H. Koenig, C.M. Baglin, R.D. Brown, Magnetic field dependence of solvent proton relaxation in aqueous solutions of Fe3+ complexes, *Magn. Reson. Med.* 2 (1985) 283–288.
- [39] S.H. Koenig, R.D. Brown, J.F. Gibson, R.J. Ward, T.J. Peters, Relaxometry of ferritin solutions and the influence of the Fe3+ core ions, *Magn. Reson. Med.* 3 (1986) 755–767.
- [40] R.S. Desikan, F. Segone, B. Fischl, B.T. Quinn, B.C. Dickerson, D. Blacker, R. L. Buckner, et al., An automated labeling system for subdividing the human cerebral cortex on MRI scans into gyral based regions of interest, *Neuroimage* 31 (3) (2006) 968–980.
- [41] H.J. Johnson, G. Harris, K. Williams, BRAINSFit: mutual information registrations of whole-brain 3D images, using the insight toolkit, *The Insight Journal* (2007) 180.
- [42] J.C. Moser, M. Rawal, B.A. Wagner, J. Du, J.J. Cullen, G.R. Buettner, Pharmacological ascorbate and ionizing radiation (IR) increase labile iron in pancreatic cancer, *Redox Biol. Elsevier* 2 (2013) 22–27.
- [43] F.E. Harrell Jr., R.M. Califf, D.B. Pryor, K.L. Lee, R.A. Rosati, Evaluating the yield of medical tests, *J. Am. Med. Assoc.* 247 (1982) 2543–2546.
- [44] M. Schmid, M.N. Wright, A. Ziegler, On the use of Harrell's C for clinical risk prediction via random survival forests, *Expert Syst. Appl.* 63 (2016) 450–459.
- [45] O. Dietrich, J. Levin, S.-A. Ahmadi, A. Plate, M.F. Reiser, K. Bötzel, et al., MR imaging differentiation of Fe2+ and Fe3+ based on relaxation and magnetic susceptibility properties, *Neuroradiology* 59 (2017) 403–409.